Static instability of an asymmetrical two-layered beam supported by a Pasternak base under thermal gradient and an axial pulsating load

Madhusmita Pradhan[1], *Madhumita* Mohanty[2*], *Sasmita* Sahu[2], *Nabakishor* Dang[1], and *Pusparaj* Dash[1]

[1]Department of Mechanical Engineering, Veer Surendra Sai University of Technology, Burla, India
[2]School of Mechanical Engineering, Kalinga Institute of Industrial Technology, Bhubaneswar, India

Abstract. This study focuses on lightweight structural components that are commonly used in mechanical, marine, and aerospace systems where achieving high strength at low weight is a key design objective. The suggested beam in this analysis eliminates the need for a viscoelastic core and achieves reduced mass without sacrificing stiffness by bonding two dissimilar elastic materials together. To simulate actual operating conditions, the model is exposed to a thermal gradient and an axial pulsating load. The governing non-dimensional Hamilton's concept is used to generate equations and the related boundary conditions, and Galerkin's approach further streamlines them for computational use. For both pinned & pinned and clamped & pinned edge conditions, the impact of geometric ratios, elastic modulus variation, taper characteristics, foundation rigidity, and thermal effects is examined. The effect of these parameters on the beam's static stability is evident from numerical results derived from MATLAB simulations.

1 Introduction

Composite and multilayer beam structures can combine low weight with high stiffness and strength, they have become increasingly important in modern engineering design. Among different structural arrangements, a two-layer elastic beam provides a more straightforward and effective substitute for traditional sandwich beams, which are made of two dissimilar materials that are bonded together to produce the required mechanical performance. Compared to the conventional Winkler foundation, the Pasternak foundation model offers a more accurate depiction of elastic support conditions since it takes into consideration both vertical spring stiffness and inter-layer shear interaction. The present investigation examines the static stability of a beam with two layers with an asymmetrical taper that is subjected to an axial pulsing load and a temperature gradient while being supported by a variable Pasternak foundation. In mechanical, aerospace, and civil structures where dynamic excitation and thermal stress coexist, such loading conditions are common. Galerkin's approach is utilised to generate the governing Hill-type calculation, and the system is

* Corresponding author: madhumita.mohanty92@gmail.com

formally formulated using Hamilton's energy principle. The effects of foundation stiffness, tapering, material modulus ratio, and geometric ratios on the critical buckling load are evaluated numerically. An important way to understand how edge conditions affect overall stability is to compare clamped-pinned and pinned-pinned boundaries.

1.1 Nomenclature

A1: Top layer cross-section area	γ_e =Elastic foundation parameter
A2: Bottom layer cross-section area	E21 =E2 /E1
E1: Top layer material modulus of Elasticity	$l_{h1} = l/h_1$
E2: Bottom layer material modulus of Elasticity	$\lambda_s = kl/E1$
c: h1 + h2	
α_1, α_2 = Taper Parameter	
d: Shear layer thickness in foundation	
Gs: Pasternak foundation shear layer rigidity Modulus	
P0: Amplitude for static load	
k: Stiffness of Pasternak Foundation spring	
$\omega =$ Frequency of axial pulsating load	
$\bar{\omega} = \omega t_0$ = Non-dimensional frequency ratio	
P_1: Dynamic load amplitude	

1.2 Material properties

The topmost part of the two-layered beam in this study is made of aluminium alloy, while the Structural steel makes up the bottom layer. The proper bonding adhesive is used to join these materials. Table 1 lists their mechanical characteristics.

Table 1. Mechanical properties of material.

Material Name/ property	**Density** (kg/m^3)	**Ultimate Tensile Strength [Pascal]**	**Young's Modulus [Pascal]**
Structural Steel	7850	4.6×10^{8}	2×10^{11}
Aluminium alloy	2770	3.1×10^{8}	7.1×10^{10}

1.3 Literature review

Much research has been done on the stability and vibration analysis of sandwich and layered beams. In their investigation of the instability properties of multilayer sandwich beams, Ray and Kar [1] showed how interlayer interaction affects dynamic performance. Asymmetric sandwich beams supported by Pasternak foundations were examined by Dash et al. [2], who found that stability limits are greatly impacted by foundation stiffness. In order to investigate the vibration response of two-layer Timoshenko beams under different boundary constraints, Song et al. [3] used a spectral element technique. Similar to this, Smyczynski and Magnucka-Blandzi [4] examined the axial load's impact on buckling resistance while examining the static and dynamic stability of axially compressed multilayer beams. The effects of inertia, interface characteristics, and shear stiffness on the vibration frequencies of layered beams were examined by Lenci and Clementi [5]. In their study of two-layer elastic beams supported on variable Pasternak foundations, Mohanty et al. [6] emphasised the importance of foundation parameters in vibration control. Later, this work was expanded to include nonlinear vibration responses under various boundary conditions by Lenci et al. [7]. Additionally, Mohanty et al. [8] investigated the parametric instability of two-layer beams on uneven foundations, emphasising the impact of stiffness and taper variation. While Nayak et al. [10] conducted dynamic stability studies on magnetorheological sandwich beams under specific boundary conditions, Aytac and Ibrahim [9] used the differential transform method to analyse composite sandwich beams with viscoelastic cores.

It is clear from the review of the literature that, although there are a lot of studies on dynamic and vibration behaviour, the static stability of asymmetrically tapered two-layer beams subjected to both axial and thermal effects has received little attention. By creating a methodical research that measures how temperature gradients affect structural ratios, Pasternak base factors affect the critical buckling load under two boundary configurations, the current work seeks to close this gap.

2 Mathematical formulation

The beam model consists of an aluminium top layer and a steel bottom layer, each tapering along the length *l*. The system rests on a variable Pasternak foundation characterized by vertical springs of stiffness *k* and a shear layer of thickness *d* and modulus *Gs* as shown by Figure 1. The beam is subjected to an axial pulsating load expressed as:

$$P_P(t) = P_0 + P_1 \cos(\omega t)$$

Key assumptions include:

- Small transverse deflection and continuity across layers.
- Both layers follow Euler–Bernoulli beam theory.
- The Pasternak shear layer resists shear without undergoing extensional deformation.
- Rotary inertia effects are neglected.

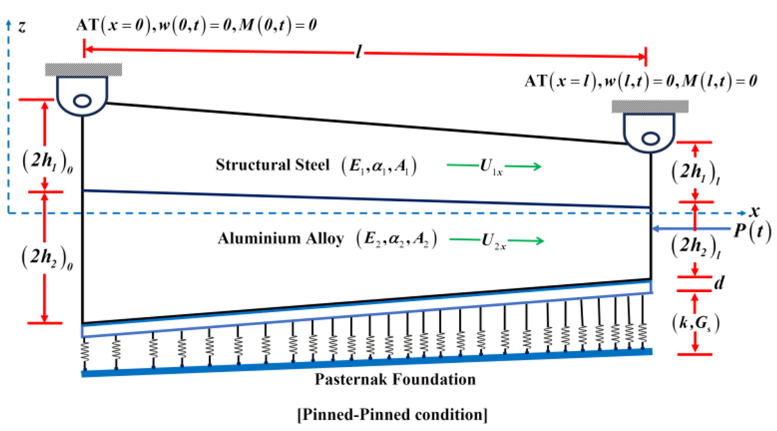

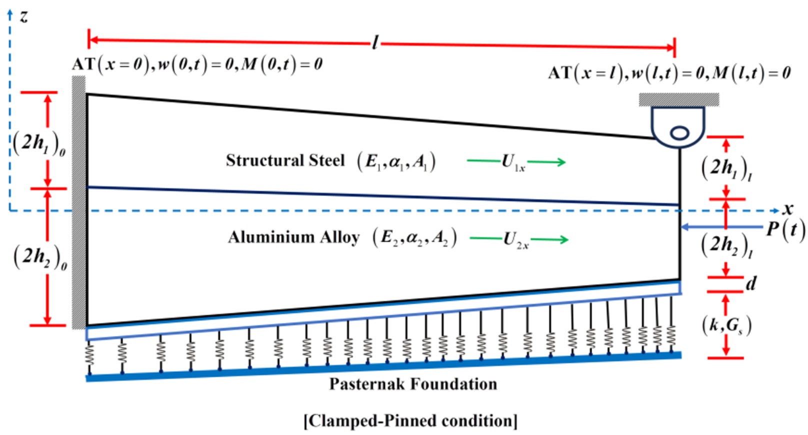

Fig. 1. System configuration.

The corresponding energy of the system i.e., potential energy (V),

$$V_E = \frac{1}{2}E_1A_1\int_0^l U_{1,x}^2 + \frac{1}{2}E_2A_2\int_0^l U_{2,x}^2 + \frac{1}{2}(E_1I_1 + E_2I_2)\int_0^l ww_{xx}^2dx + \frac{1}{2}G_sbd\int_0^l ww_x^2dx + \frac{kb}{2}\int_0^1 ww^2dx \tag{1}$$

kinetic energy (T),

$$T_E = \frac{1}{2}m_m\int_0^l ww_t^2dx \tag{2}$$

and work done (Wp) can be obtained by,

$$W_p = \frac{1}{2}\int_0^l P_p(t)ww_x^2dx \tag{3}$$

U_1 : Top face displacement, U_2 : Bottom face displacement.

$ww_{,x} = \frac{\partial ww}{\partial x}$, $ww_{,t} = \frac{\partial ww}{\partial t}$

Using equation (01), (02) and (03), Hamilton's Principle is applied as:

$$\delta\int_{t_1}^{t_2}(T_E - V_E + W_p)dt = 0 \tag{4}$$

$$\overline{m}_m(\overline{ww}_{,\overline{tt}}) + (1+Y)\overline{ww}_{,\overline{xxxx}} - \left[\frac{3}{2}\frac{G_s}{E_1}\frac{d}{l}\frac{(lh_{10})^3}{1+E_{21}h_{21}{}^3} - P_P(\overline{t})\right]\overline{ww}_{,\overline{xx}} + \frac{3}{2}\times\frac{k(x)\times l}{E_1}\frac{(lh_{10})^3}{1+E_{21}h_{21}{}^3}\overline{ww} = 0 \tag{5}$$

Equation 5 is showing the non-dimensioned equation of motion.

Where,

$$c=(h_1)_l+(h_2)_l,\ \overline{ww}_{\overline{xxxx}}=\frac{\partial^4\overline{ww}}{\partial\overline{x}^4},\ \overline{ww}_{\overline{xx}}=\frac{\partial^2\overline{ww}}{\partial\overline{x}^2}$$

$$\overline{ww}=ww/l,\overline{x}=x/l,\ t_0=[(\rho_1)(A_1)_0 l^4/E_1(I_1)_0]^{1/2},\ \overline{P}_P=Pl^2/\{E_1(I_1)_0\}=\overline{P}_0+\overline{P}_1\cos(\overline{\omega}\overline{t})$$

$$\overline{P}_0=\frac{P_0l^2}{E_1(I_1)_0},\ \overline{P}_1=\frac{P_1l^2}{E_1(I_1)_0},\ \overline{\omega}=\omega t_0,\ \overline{U}=U/l,\ \overline{t}=t/t_0$$

Various parameters, which are section-dependent as

$$\overline{m}_m=(1-\overline{x})+\left[\frac{(h_2)_l}{(h_1)_0}\right]\left(\frac{\rho_2}{\rho_1}\right)\overline{x},\ Y=\frac{3(1-\overline{x}\alpha_1)(1+2\beta+h_{21})^2}{\left[(1+\alpha)[(1-\overline{x}\alpha_1)^3+\frac{E_2}{E_1}h_{21}(1-\overline{x}\alpha_2)^3\right]},$$

$$\alpha_1=\frac{1}{(h_1)_0}\times(h_1)_0-(h_1)_l,\ \alpha_2=\frac{1}{(h_2)_0}\times(h_2)_0-(h_2)_l,\ \beta=\frac{(h_2)_0}{(h_1)_0},\ \mu_1=\frac{\rho_2}{\rho_1}$$

$(I_1)_0$= Top layer moment of inertia at the left end
$(A_1)_0$= Top layer cross-section area at the left end
boundary conditions for the system are at $\overline{x}=0$, and $\overline{x}=1$,

$$(1+Y)\overline{ww}_{,\overline{xxx}}-\left[\frac{3}{2}\frac{G_s d(lh_{10})^3}{(1+E_{21}h_{21}{}^3)}-\overline{P}_P(\overline{t})\right]\times ww_{,\overline{x}}=0 \quad \text{or} \quad \overline{ww}=0 \tag{6}$$

$$(1+Y)ww_{,\overline{xx}}=0 \quad \text{or} \quad \overline{ww}_{,\overline{x}}=0 \tag{7}$$

The estimated solutions are

$$\overline{ww}=\sum_{ii=1}^{ii=P}ww_{ii}(\overline{x})f_{ii}(\overline{t}) \tag{8}$$

$$\overline{U}=\sum_{kk=P+1}^{kk=2P}U_{kk}(\overline{x})f_{kk}(\overline{t}) \tag{9}$$

w, U are coordinate functions, and the generalised Coordinates are f_{ii}, f_{kk}. $ww_{ii}(\overline{x}_{ii}),\ U_{kk}(\overline{x}_{kk})$ are selected to satisfy the maximum possible boundary conditions. The shape

Shape function for Pinned-Pinned:

$$ww_{ii}(\overline{x})=\sin(ii\pi\overline{x}) \tag{10}$$

$$\overline{U}_{kk}(\overline{x})=\cos(kk\pi\overline{x}) \tag{11}$$

Again Clamped-pinned:

$$ww_{ii}(\overline{x})=2(ii+2)\overline{x}^{(ii+1)}-(4ii-6)\overline{x}^{(ii+2)}+2(ii+1)\overline{x}^{(ii+3)} \tag{12}$$

$$\overline{U}_{kk}(\overline{x})=(\overline{kk}+1)\overline{x}^{kk}-\overline{kk}\overline{x}^{(kk+1)}\text{, where } \overline{kk}=kk-P \tag{13}$$

The shape functions are applied in equations (08) and (09).

The Generalised Galerkin technique is used to transform the equation of motion into matrix form, as follows,

$$\left[M_M\right]\{\ddot{Q}_1\}+\left[K_{K11}\right]\{Q_1\}+\left[K_{K12}\right]\{Q_2\}=\{0\} \tag{14}$$

$$\left[K_{K12}\right]^{T}\{Q_1\}+\left[K_{K22}\right]\{Q_2\}=\{0\} \tag{15}$$

The different matrix elements are

$$M_{ij}=\int_0^1 \overline{m}ww_i ww_j d\overline{x} \tag{16}$$

$$K_{K11ij}=(1+Y)\int_0^1 ww_i'' ww_j'' dx+\phi\int_0^1 ww_i ww_j dx+[\psi-\overline{P}(\overline{t})]\int_0^1 ww_i' ww_j' dx \tag{17}$$

$$K_{K12jk}=Y\int_0^1 ww_i'' U_k' dx \tag{18}$$

$$\lambda_s=\frac{kl}{E_1},\phi=\frac{3\lambda_s(lh_{10})^3}{2(1+E_{21}h_{21}{}^3)},\psi=\frac{3G_s d(lh_{10})^3}{2E_1 l(1+E_{21}h_{21}{}^3)},[K_{K21}]=[K_{K12}]^T$$

$$\left[M_M\right]\{\ddot{Q}_1\}+[[K_k]-\overline{P}_0[H]]\{Q_1\}-\overline{P}_1\cos(\omega t)\left[H\right]\{Q_1\}=\{0\} \tag{19}$$

Here,

$$\left[K_K\right]=[\overline{K}_K]-\left[K_{K12}\right]\times\frac{1}{\left[K_{K22}\right]}\times\left[K_{K12}\right]^T$$

$$H_{iijj}=\int_0^1 (w_{ii})'(w_{jj})'d\overline{x}$$

$$[\overline{K}_{ij}]=(1+Y)\int_0^1 ww_i'' ww_j'' d\overline{x}+\phi\int_0^1 ww_i ww_j d\overline{x}+\psi\int_0^1 ww_i' ww_j' d\overline{x}$$

2.1 Static buckling load

Substituting $\overline{P}_1=0$ and $\{\ddot{Q}_1\}=0$ in equation (19) gives $[K_K]^{-1}[H]\{Q_1\}=\frac{1}{P_0}\{Q_1\}$.
The load acting for the static buckling of the system is taken as the real parts of the eigenvalue's reciprocal. The elastic foundation is considered with the stiffness as, $K_K(\overline{x})=\{1+4(1-\gamma_e)\times(\overline{x}^2-\overline{x})\}$, which is parabolic in nature, γ_e represents the elastic foundation parameter.

2.2 Thermal gradient analysis

The temperature of the beam is assumed to be $\psi=\psi_0(1-\xi)$ at some point ξ from left end of the beam above the reference temperature.

Considering $\psi_0=\psi_1$ and, $\xi=1$ as the reference temperature, the young's modulus of elasticity varies asz

$$E(\xi)=E_1[1-\gamma\psi_1(1-\xi)],\ 0\le\gamma\psi_1<1$$
$$=E_1T(\xi) \tag{20}$$

Here γ represents the thermal expansion co-efficient for beam material of the beam, $(P_0)_{cri}$ thermal gradient parameter, and $T(\xi) = [1 - \delta(1-\xi)]$.

$$\alpha = \frac{E_1 A_1}{E_2 A_2} = \frac{E_1 T(\xi)}{E_2 T(\xi)} \times \frac{A_1}{A_2}$$

3 Results

The investigation was performed by varying parameters, including the thermal gradient, elastic modulus ratio, taper coefficient, foundation stiffness, and geometric ratios. Using MATLAB, these parameters were systematically analysed, and the corresponding numerical outcomes were illustrated through graphical representations. Figures 2 to 9 depict how each parameter influences the system's non-dimensional critical buckling load. In all the figures, the blue solid line corresponds to the clamped–pinned boundary condition, while the red solid line represents the pinned–pinned boundary configuration. Table 2 shows the different parameter values used for static stability analysis.

Table 2. Parameter values for static analysis.

Parameter	value	Parameter	value
l	160	P_0	0.0005
G_S/E_1	0.002	b	20
α_1	0.002	d	5
α_2	0.002	ρ_1/ρ_2	0.35
E_2/E_1	2.0		
δ_1	0.3		
δ_1	0.3		

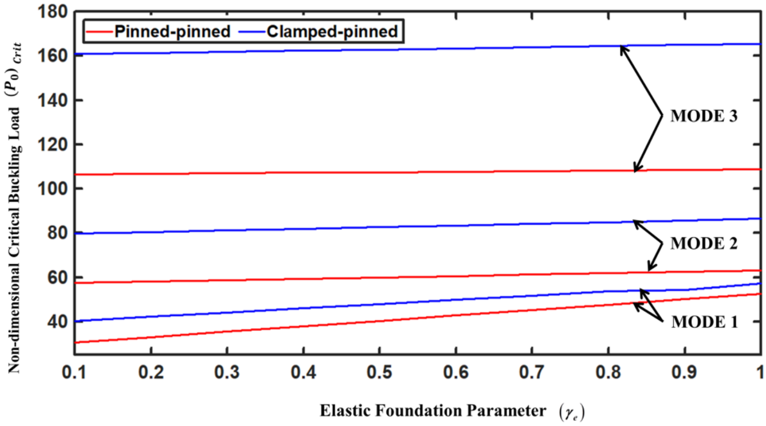

Fig. 2. Effect of γ_e on $(P_0)_{cri}$.

Figure 2 demonstrates that as the foundation parameter γ_e increases, the associated critical buckling load increases gradually. This pattern suggests that increased resistance to buckling and improved structural rigidity are facilitated by a more rigid supporting foundation. Thus, increasing γ_e results in greater overall static stability.

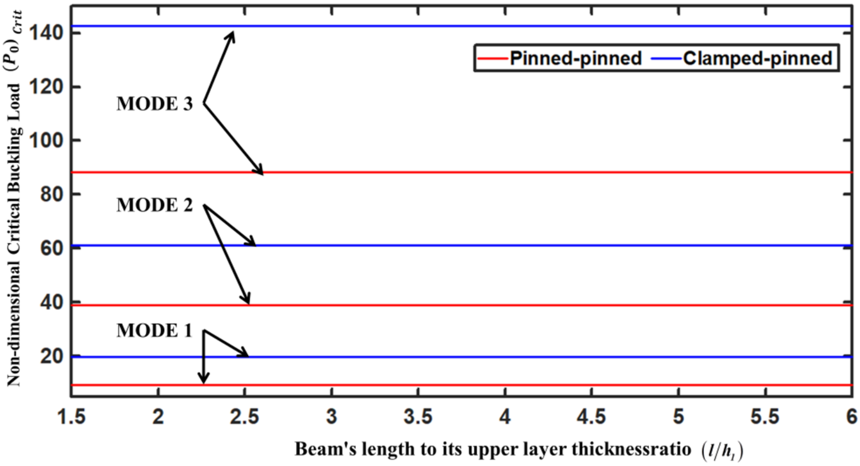

Fig. 3. Effect of l/h_1 on $(P_0)_{cri}$.

The distribution of stiffness is significantly influenced by the ratio of the beam's length to its upper layer thickness (l/h_1). Figure 3 indicates that increasing this ratio strengthens the beam and enhances its load-carrying capacity because the critical buckling load increases moderately with larger values.

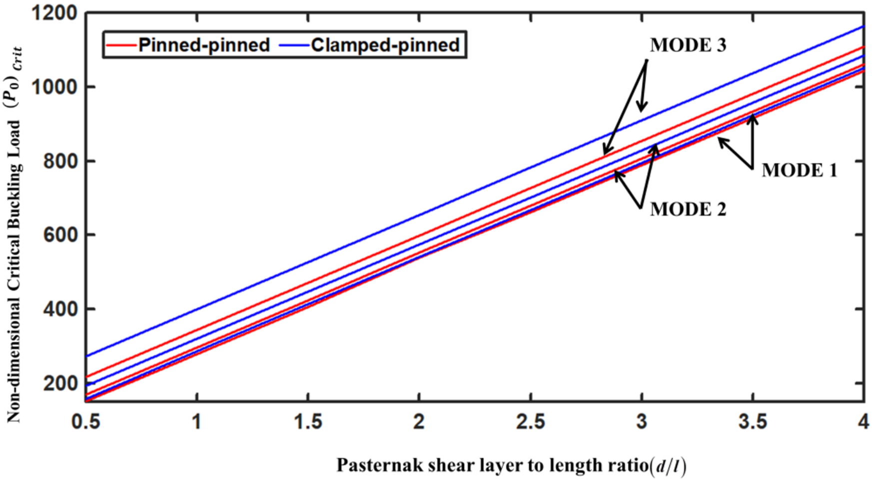

Fig. 4. Effect of d/l on $(P_0)_{cri}$.

Figure 4 shows that there is a positive correlation between the parameter and the critical buckling load. The structure obtains more shear resistance through the Pasternak layer as the relative shear-layer thickness rises, improving the static stability across all boundary configurations and vibration modes taken into consideration.

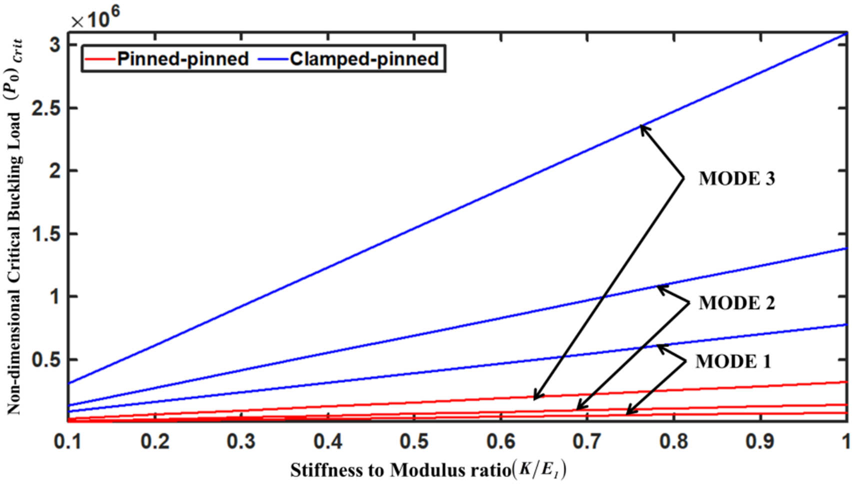

Fig. 5. Effect of K/E_1 on $(P_0)_{cri}$.

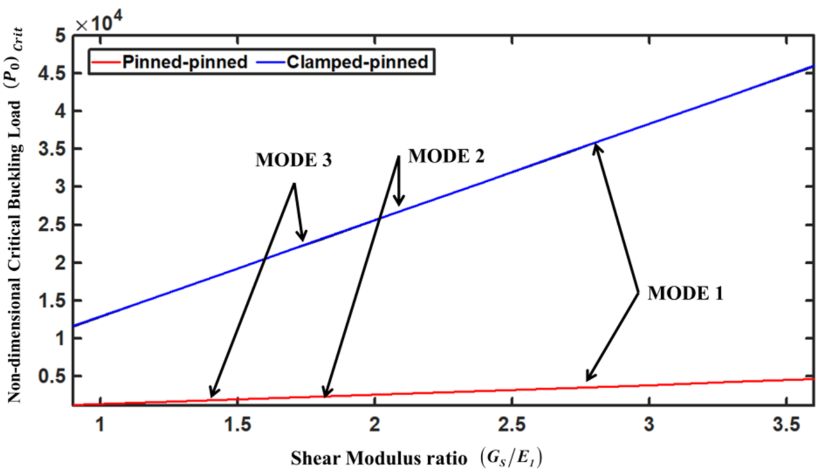

Fig. 6. Effect of G_s/E_1 on $(P_0)_{cri}$

Figures 5 and 6 illustrate how both the spring stiffness-to-modulus ratio (K/E_1) and the shear modulus ratio (G_s/E_1) influence the buckling characteristics. The critical buckling load rises noticeably in each scenario as these ratios increase. This illustrates how the ability of the beam to tolerate axial compression without losing stability is greatly increased by materials with greater stiffness or shear resistance. The same pattern is found for (K/E_2) and (G_s/E_2), but they are omitted here for brevity.

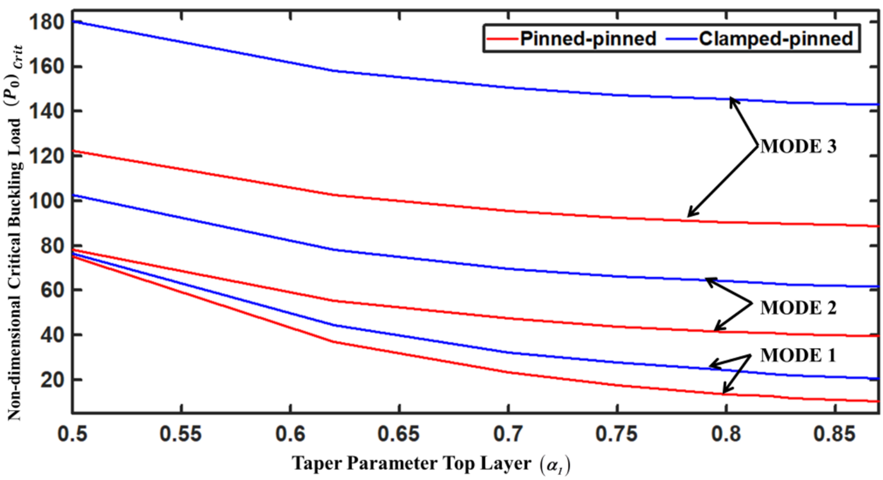

Fig. 7. Effect of α_1 on $(P_0)_{cri}$.

Figure 7 highlights the impact of tapering on structural stability. As α_1 increases, the beam becomes more non-uniform in thickness, resulting in reduced stiffness toward the free end. Consequently, the critical buckling load decreases, signifying a decline in static stability. Similar observations hold for α_2, though its plot is not included to avoid redundancy.

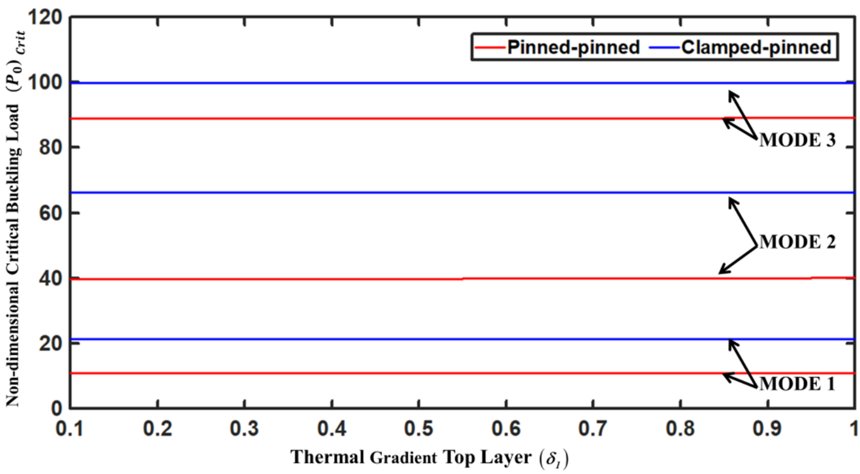

Fig. 8. Effect of δ_1 on $(P_0)_{cri}$.

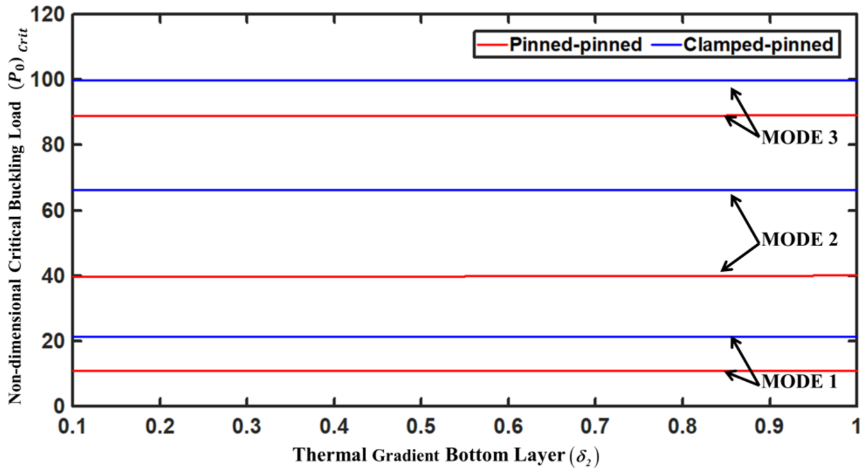

Fig. 9. Effect of δ_2 on $(P_0)_{cri}$.

Above figures 8 and 9 showing thermal gradients in the top (δ_1) and bottom layers (δ_2) ,effect on the stability of the beam respectively. A mild temperature gradient produces a slight increase in the first-mode buckling load for both pinned–pinned and clamped–pinned cases, whereas the influence on higher modes is almost negligible. This indicates that moderate thermal variation can slightly enhance stiffness by altering material elasticity, but its contribution remains secondary compared to geometric or foundation effects.

4 Conclusion

The present investigation focuses on the static stability characteristics of an asymmetric, tapering, two-layer elastic beam, that is subject to a temperature gradient and axial pulsating stress, and is supported by a variable Pasternak foundation. Two traditional boundary conditions—pinned–pinned and clamped–pinned—were examined.

The static stability is improving with a rise in the elastic foundation parameter (γ_e) , modulus ratios (k/E_1, k/E_2, Gs/E_1, and Gs/E_2), and the ratio of geometric parameters (d/l, l/h_1). But the reverse effect is observed with an increasing value of the taper parameter (α_1). The thermal gradient is affecting the system marginally by increasing the static buckling load, which enhances the stability. So, to design a statically stable system, the elastic foundation parameter, modulus ratio, and the ratio of geometric parameters should be kept high, and the taper parameter should be kept low to secure the system.

References

1. K. Ray, and R. C. Kar, Parametric instability of multi-layered sandwich beams, Journal of sound and vibration **193.3** (1996):631-644. https://doi.org/10.1006/jsvi.1996.0305
2. P. R. Dash, B. B. Maharathi, and K. Ray, Dynamic Stability of an Asymmetric Sandwich Beam Resting on a Pasternak Foundation, Journal of Aerospace Science and Technologies **62.1** (2010): 66. https://doi.org/10.61653/joast.v62i1.2010.488
3. S. Lenci, and C. Francesco, Effects of shear stiffness, rotatory and axial inertia, and interface stiffness on free vibrations of a two-layer beam, Journal of Sound and

Vibration **331.24** (2012): 5247-5267, https://doi.org/10.1016/j.jsv.2012.07.004

4. M. J. Smyczynski and E. Magnucka-Blandzi. Static and dynamic stability of an axially compressed five-layer sandwich beam., Thin-Walled Structures **90** (2015): 23-30.https://doi.org/10.1016/j.tws.2015.01.005
5. S.Younghoon, S. Kim, I. Park, U. Lee. Dynamics of two-layer smart composite Timoshenko beams: frequency domain spectral element analysis, Thin-Walled Structures **89** (2015): 84-92, https://doi.org/10.1016/j.tws.2014.12.016
6. M. Mohanty, S. Bhattacharya, S. Yadav, M. Pradhan, Free vibration analysis of a two-layer elastic beam resting on a variable Pasternak foundation, Materials Today: Proceedings **5.9.3** (2018):19242-19240. https://doi.org/10.1016/j.matpr.2018.06.281
7. L. Stefano, C. Francesco, W. Jerzy, Nonlinear free dynamics of a two-layer composite beam with different boundary conditions. Meccanica 2015; **50(3):**675–688. DOI 10.1007/s11012-014-9945-6
8. M. Mohanty, M. Pradhan, R. Mishra, Stability analysis of a two-layer elastic beam resting on a variable Pasternak foundation subjected to an axial pulsating load and thermal gradient. *Materials Today: Proceedings* **5.11** (2018): 23619-23628.https://doi.org/10.1016/j.matpr.2018.10.151
9. A Aytac, O. Ibrahim, Vibration analysis of composite sandwich beams with viscoelastic core by using the differential transform method, Composite Structures, 2010;**92(12)**:3031–9. https://doi.org/10.1016/j.compstruct.2010.05.022
10. B. Nayak, S. K. Dwivedy, and K. S. R. K. Murthy, Dynamic analysis of magnetorheological elastomer-based sandwich beam with conductive skins under various boundary conditions, Journal of Sound and Vibration **330.9** (2011): 1837-1859. https://doi.org/10.1016/j.jsv.2010.10.041